Journal of The Electrochemical Society, **150** (1) E11-E16 (2003)
0013-4651/2002/150(1)/E11/6/$7.00 © The Electrochemical Society, Inc.

Effect of Electrolyte Flow on the Bubble Coverage of Vertical Gas-Evolving Electrodes

R. J. Balzer[a] **and H. Vogt**[z]

Laboratory for Reaction Technology, Technische Fachhochschule, Berlin-University of Applied Sciences, D-13353 Berlin, Germany

The bubble coverage of vertical gas-evolving electrodes with forced upward electrolyte flow is studied systematically in laboratory experiments. A substantial decrease with increasing flow velocity past the electrode is found for various electrode materials of anodes and cathodes. A theoretical analysis explains the action of mechanical forces on the break-off diameter of bubbles exposed to flowing electrolytes. A simplified design equation for practical estimates is proposed.
© 2002 The Electrochemical Society. [DOI: 10.1149/1.1524185] All rights reserved.

Manuscript submitted April 10, 2002; revised manuscript received June 21, 2002. Available electronically November 15, 2002.

Reliable knowledge of the electrode area covered by adhering bubbles is of utmost importance for assessing the operational behavior of gas-evolving electrodes. The value is not only relevant to the ohmic voltage drop of the so-called bubble curtain before the electrode, but also for the extent of mass and heat transfer. The bubble coverage controls the actual current density and thus both the overpotential and the limiting current density.[1] A variation of the bubble coverage with distance from the leading edge contributes to the current distribution over the electrode.

It is not astonishing that numerous experimental investigations were conducted to get information on the value of the bubble coverage, particularly its dependence on the current density. Nearly all of these investigations refer to stagnant electrolyte, *i.e.*, liquids without forced flow, mostly in experimental devices where substantial flow past the electrode cannot develop. However, industrial cells are commonly operated with forced upward flow or designed in such a way that substantial free flow induced by gas bubbles develops. Owing to experimental difficulties, data under these conditions are rare. A few data were published by Sillen obtained at a cell with vertical electrodes.[2,3] More detailed data were obtained at horizontal electrodes facing upward.[4] However, industrial gas-evolving electrodes are in a vertical position, wherever possible, to enhance gas release from the interelectrode space. It is the object of the present paper to study the conditions at vertical electrodes of various electrode materials operated as anodes and cathodes with forced flow of varying rates.

Bubble Coverage in Stagnant Liquids

To distinguish the active electrode surface area from the geometrical one, the (fractional) bubble coverage was introduced by Ibl and Venczel[5] in 1961. It was defined as the fraction of the electrode area covered on the average by bubbles sitting on it. A stricter definition was given in 1980 defining the covered area as that obtained by perpendicular projection of the bubble contours to the electrode, referred to the electrode mean area pertinent to each adhering bubble.[6] This definition is superior in that it considers that the current density on the shadowed area below adhering bubbles with contact angles smaller than 90° (which is a common case in aqueous electrolytes) is small,[7-9] and may approximately be neglected for the present purpose.

The value of the bubble coverage is controlled by the bubble population density on the electrode surface, *i.e.*, the number z of simultaneously existing bubbles on the surface area A, and by the velocity of bubble growth reflected by the average shadowed area during the average residence time of bubbles at the surface, t_r. With the radius R of a representative bubble the bubble coverage is

$$\Theta \equiv \frac{z}{A t_r} \int_0^{t_r} \pi (K_1 R)^2 dt \qquad [1]$$

where K_1 is a geometric parameter depending on the contact angle with[4,10]

$$K_1 = 1 \quad \text{for} \quad \vartheta \leqslant 90° \qquad K_1 = \sin \vartheta \quad \text{for} \quad \vartheta \geqslant 90°$$

As bubbles adhering to the electrode surface grow by diffusion, the radius increases with the root of time. Then, Eq. 1 results in

$$\Theta = \frac{\pi}{2} \frac{z}{A} (K_1 R_r)^2 \qquad [2]$$

where R_r denotes the radius of the detaching bubble at $t = t_r$.

Active nucleation sites are small surface irregularities the geometry of which enables a tiny gas rest to grow by supply of dissolved gas from the surrounding liquid if the supersaturation is sufficiently large. The number of nucleation sites on the electrode surface is largely affected by the microstructure of the surface, hence by the kind of material, its condition and roughness, and it is further affected by wettability, which, in turn, is the result of the interfacial tensions of the three-phase system electrode/electrolyte liquid/gas. The supersaturation is controlled by the current density and by the two competing mass transfer mechanisms, *i.e.*, the transfer of dissolved gas from the electrode to the bulk of liquid and the transfer from the environs of the adhering bubble to the gas/liquid interface. The complexity of these effects cannot be quantitatively described satisfactorily at present.

But it is generally agreed that in stagnant liquids, *i.e.*, in absence of forced liquid flow, the mechanism of microconvective mass transfer in the vicinity of growing bubbles predominates. The velocity of bubble growth may then approximately be related directly to the current density.[6] A compilation of numerous experimental data from several workers[2,5,11-19] is shown in Fig. 1 and can tentatively be correlated by

$$\Theta_0 = 0.023 \left(\frac{I/A}{\mathrm{Am}^{-2}} \right)^{0.3} \qquad [3]$$

Equation 3 is restricted to stagnant electrolyte (without forced flow or substantial natural flow) and mostly to smooth bubble release, but provides a useful design equation for practical purposes. In contrast, cells with horizontal electrode surfaces facing downward, as used in the Hall-Héroult process, exhibit large values of the bubble coverage even at modest nominal current densities.[20,21]

Theory of Flowing Electrolytes

In stagnant liquids, bubbles detach from a horizontal electrode surface facing upward, when the adhesion force is exceeded by the difference of buoyancy force and gravitational force. In flowing liquids, an additional drag force enhances detachment. This drag force

[a] Present address: Edelstahlwerke Buderus AG, Wetzlar, Germany.
[z] E-mail: helmutvogt@uni.de

Downloaded on 2015-06-26 to IP 132.236.27.111 address. Redistribution subject to ECS terms of use (see ecsdl.org/site/terms_use) unless CC License in place (see abstract).

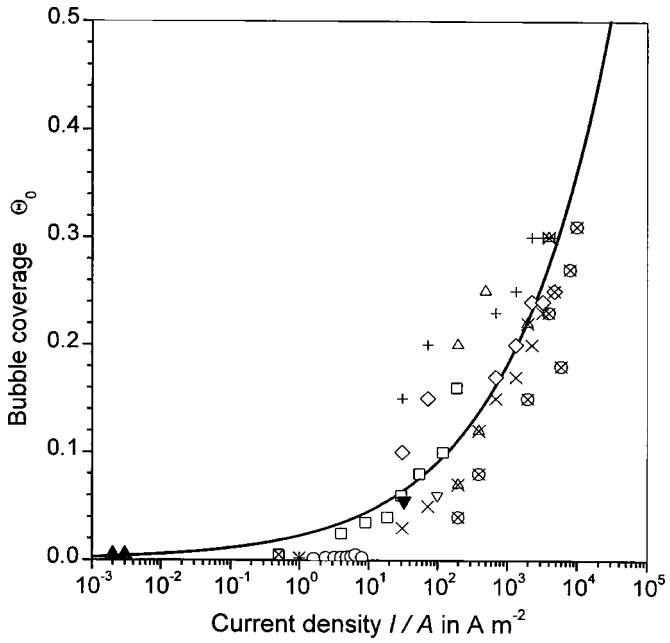

Figure 1. Bubble coverage as a function of the current density. Evolution of hydrogen, chlorine, and oxygen from stagnant aqueous electrolyte liquids (aqueous solutions of KOH, HCl, H_2SO_4) at various electrode materials (Ni, Pt, Cu, C, Pb, Hg) according to various workers[2,5,11–19] and data from present work. Temperature 20-30°C, ambient pressure.

depends on the flow velocity of the liquid and the channel geometry. At vertical electrodes with upward flow of electrolyte liquid past the electrode surface, as treated here, the buoyancy force and gravitational force

$$F_1 = Vg(\rho_L - \rho_G) \quad [4]$$

the drag force[22]

$$F_2 = \zeta\rho_L \frac{v^{*2}}{2}\pi R^2\left(1 - \frac{\vartheta - \cos\vartheta\sin\vartheta}{\pi}\right) \quad [5]$$

and the interfacial tension force

$$F_3 = 2\pi R\sin\vartheta\gamma(\cos\vartheta_r - \cos\vartheta_a)K_2 \quad [6]$$

act on an adhering bubble of radius R. V denotes the actual volume of the gas bubble adhering to the surface. All forces act parallel to the electrode surface.

When the sum of the first two forces exceeds the third one, the bubble moves from its nucleation site upward in contact with the electrode surface and soon strikes another bubble adhering to the electrode. When the moving bubble meets the obstacle it is either diverted toward the interior of the liquid or coalesces with the encountered bubble. In both cases, the bubble leaves the electrode surface. The bubble volume at detachment from the electrode is set equal to the equivalent volume of a sphere of diameter d. Hence, this break-off diameter d is determined by the equilibrium of the three forces

$$F_1 + F_2 - F_3 = 0 \quad [7]$$

ϑ_a and ϑ_r in Eq. 6 denote the advancing and the receding angle, respectively, of the bubble adhering to the electrode surface. If the bubble is very small (and the drag force is correspondingly small), both angles are nearly equal. As the bubble increases in size, both the buoyancy force and the drag force increase, and the bubble deforms. The term in brackets on the right hand side ($\cos\vartheta_r - \cos\vartheta_a$) increases. A sufficiently simple general expression is

$$\cos\vartheta_r - \cos\vartheta_a = \left(\frac{F_1 + F_2}{C_1}\right)^m \quad [8]$$

where C_1 and m are empirical values.

The flow past industrial electrodes is mostly turbulent, particularly because of cross flow induced by bubbles adhering to the electrode. Then the drag number ζ may be set approximately independent of the velocity. The flow velocity v^* is an average value and equals approximately a distance from the electrode surface of $y = R$. The flow profile in a rectangular sectional area in turbulent flow may be correlated for small distances by

$$\frac{v^*}{v_{max}} = 1.4\left(\frac{v}{Y}\right)^{0.25} \quad [9]$$

where v_{max} denotes the maximum velocity of the profile, Y is the interelectrode distance or electrode-membrane distance. With the average value in the cross-sectional area, $\overline{v}$, follows

$$\frac{v^*}{\overline{v}} \approx \frac{v^*}{0.89v_{max}} = 1.57\left(\frac{v}{Y}\right)^{0.25} \quad [10]$$

At horizontal electrodes, the drag force is exerted essentially by the velocity of forced flow. In the present case of vertical position of the electrode, an additional velocity component induced by free flow is active. It is well-known that gas bubbles evolved at electrodes are not distributed equally in the interelectrode gap as formerly supposed for simplification, but form a layer near the electrode strongly enriched with gas, the so-called bubble curtain. The reduced effective density of the dispersion induces a natural flow superimposed on forced flow. The resulting velocities can attain large values at industrial current densities and substantially enhance electrolyte motion near the electrode forming the channel wall. The extent of free convection depends on the current density as observed by Ibl *et al.*, using a frit penetrated by gas instead of an electrode[23,24] and confirmed by Whitney and Tobias for gas-evolving electrodes.[25] The finding is supported both by application of mathematical models[26] and by experimental investigations in flow-through cells.[27,28] Recent flow simulations allow for a quantitative prediction of the velocity profile of bubble-induced free flow superimposed on forced flow.[29]

The effective velocity exerted to the adhering bubbles can be taken into account approximately by vector addition of both velocity components

$$\overline{v} = \sqrt{v_f^2 + v_k^2} \quad [11]$$

where v_k denotes the mean cross-sectional velocity of forced flow through the electrode-membrane gap

$$v_k = \frac{\dot{V}_L}{S} \quad [12]$$

and v_f denotes the superimposed component induced by free flow of the gas-liquid dispersion. The drag force under consideration of $y = R$ is

$$F_2 = 0.72\pi\zeta\rho_L(v_f^2 + v_k^2)\left(\frac{y}{Y}\right)^{0.5}R^2\left(1 - \frac{\vartheta - \cos\vartheta\sin\vartheta}{\pi}\right) \quad [13]$$

The balance of the three forces, Eq. 7, at the moment the bubble starts from its nucleation site at the end of the residence time with $R = R_r$ leads to a complex equation. So a less accurate expression is preferred instead of Eq. 9

$$\frac{v^*}{v_{max}} = 6\left(\frac{y}{Y}\right)^{0.5} \quad [14]$$

Downloaded on 2015-06-26 to IP 132.236.27.111 address. Redistribution subject to ECS terms of use (see ecsdl.org/site/terms_use) unless CC License in place (see abstract).

which delivers with

$$F_2 = 22.7\pi\zeta\rho_L(v_f^2 + v_k^2)\frac{y}{Y}R^2\left(1 - \frac{\vartheta - \cos\vartheta\sin\vartheta}{\pi}\right) \quad [15]$$

in the same way the easily solvable equation

$$d^3\left[1 + 68.1\zeta\frac{v_f^2 + v_k^2}{gY}\frac{\rho_L}{\rho_L - \rho_G}\left(\frac{R_r}{d}\right)^2\left(1 - \frac{\vartheta - \cos\vartheta\sin\vartheta}{\pi}\right)\right] = \frac{6}{g(\rho_L - \rho_G)}\left(2K_2 d\frac{R_r}{d}\frac{\gamma}{C_1^m}\sin\vartheta\right)^{1/(1-m)} \quad [16]$$

With the abbreviations

$$C_2 \equiv 68.1\zeta\frac{1}{gY}\frac{\rho_L}{\rho_L - \rho_G}\left(\frac{R_r}{d}\right)^2\left(1 - \frac{\vartheta - \cos\vartheta\sin\vartheta}{\pi}\right) \approx 68.1\zeta\frac{1}{gY}\left(\frac{R_r}{d}\right)^2\left(1 - \frac{\vartheta - \cos\vartheta\sin\vartheta}{\pi}\right) \quad [17]$$

$$C_3 \equiv \frac{6}{g(\rho_L - \rho_G)}\left(2K_2\frac{R_r}{d}\frac{\gamma}{C_1^m}\sin\vartheta\right)^{1/(1-m)} \quad [18]$$

the break-off diameter can simply be written

$$d = \left[\frac{C_3}{1 + C_2(v_f^2 + v_k^2)}\right]^{(1-m)/(2-3m)} \quad [19]$$

It is on hand that the bubble population density increases with the bubble coverage. Experimental data suggest a relationship[4]

$$\frac{z}{A} = \frac{\Theta^n}{C_4} \quad [20]$$

Combining Eq. 2, 19, and 20 results in the bubble coverage

$$\Theta = \left\{\frac{\pi K_1^2}{2C_4}\left(\frac{R_r}{d}\right)^2\left[\frac{C_3}{1 + C_2(v_f^2 + v_k^2)}\right]^{(1-m)/(1-1.5m)}\right\}^{1/(1-n)} \quad [21]$$

The limiting case of zero forced flow, $v_k = 0$, gives

$$\Theta_0 = \left[\frac{\pi K_1^2}{2C_4}\left(\frac{R_r}{d}\right)^2\left(\frac{C_3}{1 + C_2 v_f^2}\right)^{(1-m)/(1-1.5m)}\right]^{1/(1-n)} \quad [22]$$

and combination finally results in

$$\frac{\Theta}{\Theta_0} = \left[\frac{1 + C_2 v_f^2}{1 + C_2(v_f^2 + v_k^2)}\right]^{(1-m)/(1-1.5m)/(1-n)} \quad [23]$$

Experimental results of Sillen[2] and Eigeldinger[4] as well as the results of the present work show that the bubble population density increases approximately with the square root of the bubble coverage, $n = 0.5$. The values m and C_2 are empirical parameters. From Eq. 23, m is seen to be in the range $0 < m < 2/3$. Setting $m = 0$ would mean that the term $(\cos\vartheta_r - \cos\vartheta_a)$ is constant, as seen from Eq. 6. Although the forces F_1 and F_2 acting on the adhering bubble affects its deformation, the variation of the contact angle with the velocity, is supposed negligibly small. Again with $n = 0.5$ follows

$$\frac{\Theta}{\Theta_0} = \left(1 + \frac{v_k^2}{\frac{1}{C_2} + v_f^2}\right)^{-2} \quad [24]$$

For the limiting case of negligible free flow velocity, $v_k \gg v_f$, the equation takes the form

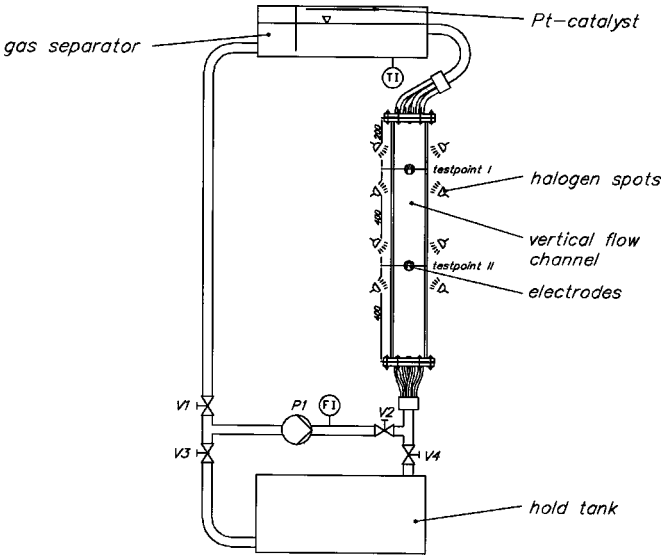

Figure 2. Experimental equipment see text for numbers.

$$\frac{\Theta}{\Theta_0} = (1 + C_2 v_k^2)^{-2} \quad [25]$$

which coincides with a previously developed fully empirical equation[4] derived for horizontal electrodes where free flow is often irrelevant.

Experimental

The experimental investigations were conducted with plane electrodes, each 40 mm in diam, made of nickel (99%), copper (99.9%), platinum-plated titanium (2.5 μm), stainless steel (X5 CrNi 18 9), and graphite. All electrodes were operated as anodes and cathodes, respectively. The electrolyte solution was an aqueous 1 M KOH solution at a temperature of 30 to 34°C and ambient pressure.

The experimental device, Fig. 2, consisted of a circulating system with vertical flow channel made of polymethylmethacrylate (130 × 10 × 1000 mm); a continuous-flow gas separator, 80 L; and a circulation pump. Forced mean flow velocity was varied from 0 to 0.9 m/s. The nominal current density was varied from 10 to 640 A m^{-2}. Prior to each run, each electrode was pre-electrolyzed for 30 min at 1000 A m^{-2}.

All working electrodes were in vertical position integrated in the wall of the flow channel at 400 and 800 mm distance, respectively, from the leading edge to investigate the effect of the flow profile. The counter electrodes were stainless steel sheets in the form of a horseshoe to prevent disturbance by bubbles evolved there.

Four halogen spots were adjusted parallel to the electrode surface to secure maximum contrast between adhering gas bubbles and the electrode surface. For each value of the current density, two pictures of bubbles at the electrode were taken with a digital camera Olympus C 2100. The picture processing program Global Lab Image 2 was used for evaluation of the shots. The program enabled digital pictures to be evaluated by means of the blob-analysis method, *i.e.*, by forming binary digits and assessment of all neighboring pixels attributed to each adhering bubble. The resulting value of the bubble coverage was obtained as arithmetic average for each couple of current density and flow velocity.

Results

The action of the flow velocity on the bubble coverage.—Experimental data points obtained for hydrogen and oxygen evolved at various electrode materials are shown in Fig. 3-6. Note that the bubble coverage decreases substantially as the velocity

Downloaded on 2015-06-26 to IP 132.236.27.111 address. Redistribution subject to ECS terms of use (see ecsdl.org/site/terms_use) unless CC License in place (see abstract).

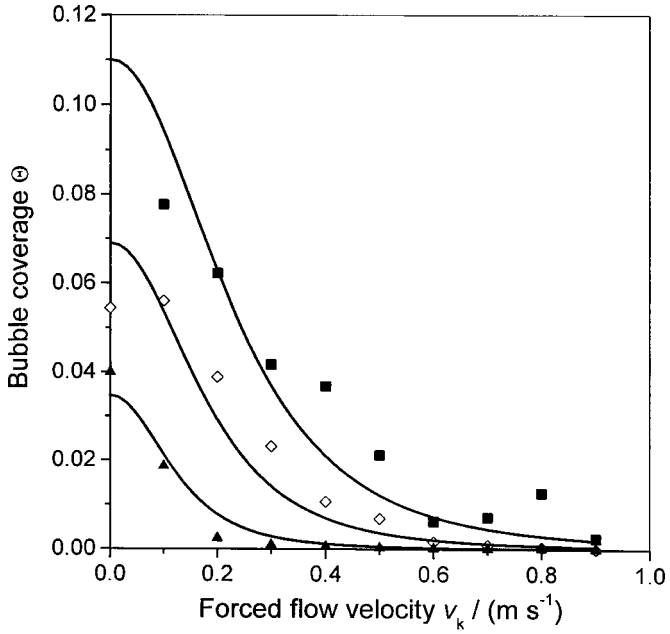

Figure 3. Effect of forced flow velocity on the bubble coverage. Hydrogen evolution at a nickel electrode; 1 M KOH at 30-34°C. (▲) 10 A m^{-2}, (◇) 20 A m^{-2}, and (■) 40 A m^{-2}. Data correlated by Eq. 28.

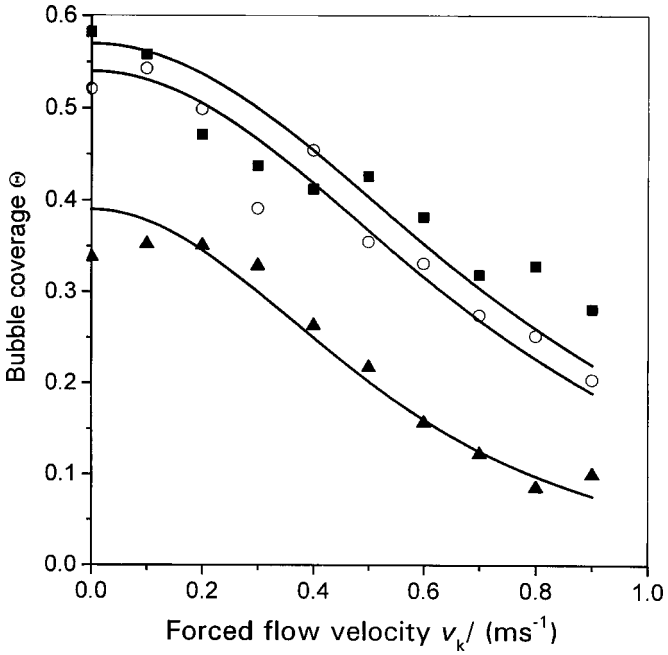

Figure 5. Effect of forced flow velocity on the bubble coverage. Oxygen evolution at a nickel electrode; 1 M KOH at 30-34°C. (▲) 10 A m^{-2}, (○) 20 A m^{-2}, (■) 40 A m^{-2}. Data correlated by Eq. 28.

of forced flow increases. Note also that comparable values of the bubble coverage of anodes are substantially larger than of cathodes and that various electrode materials affect the bubble coverage as a result of different wettability conditions.

Design equation.—The coefficient C_2 in Eq. 24 varies with the drag number ζ depending on the Reynolds number of liquid flow and on the distance between adhering bubbles, hence on the bubble coverage. It is promising to examine a dependency of C_2 on the bubble coverage. Indeed, various experimental data shown in Fig. 7 can be correlated by

$$\frac{C_2}{\mathrm{s^2 m^{-2}}} = \frac{1}{\Theta_0} - 1 \qquad [26]$$

to be used instead of a previously recommended fixed value.[4] Equation 24 takes the form

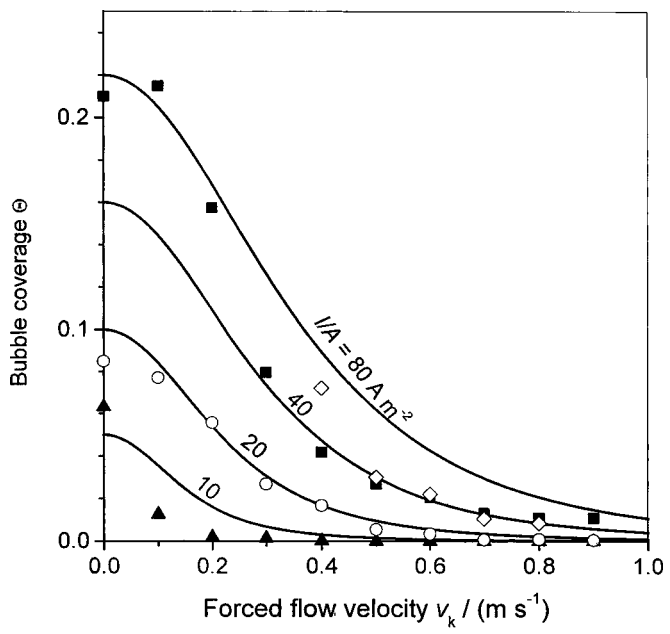

Figure 4. Effect of forced flow velocity on the bubble coverage. Hydrogen evolution at a copper electrode; 1 M KOH at 30-34°C. (▲) 10 A m^{-2}, (○) 20 A m^{-2}, (■) 40 A m^{-2}, and (◇) 80 A m^{-2}. Data correlated by Eq. 28.

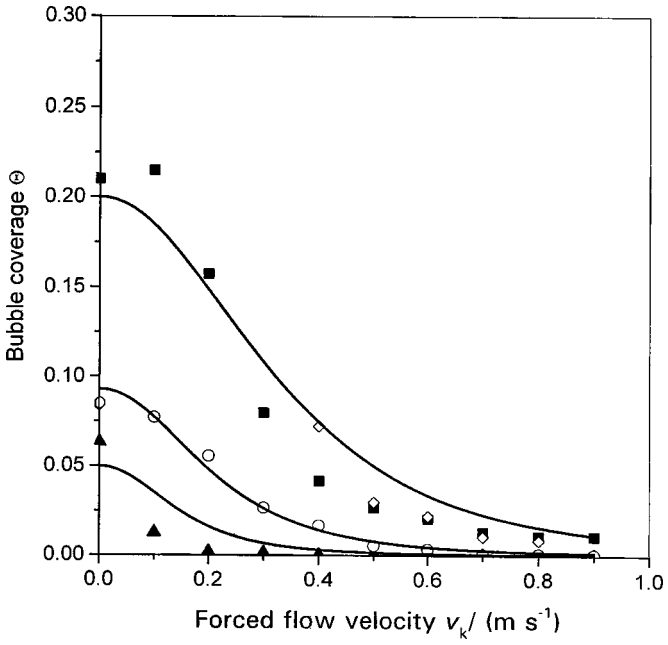

Figure 6. Effect of forced flow velocity on the bubble coverage. Oxygen evolution at a copper electrode; 1 M KOH at 30-34°C. (▲) 10 A m^{-2}, (○) 20 A m^{-2}, (■) 40 A m^{-2}, (◇) 80 A m^{-2}. Data correlated by Eq. 28.

Downloaded on 2015-06-26 to IP 132.236.27.111 address. Redistribution subject to ECS terms of use (see ecsdl.org/site/terms_use) unless CC License in place (see abstract).

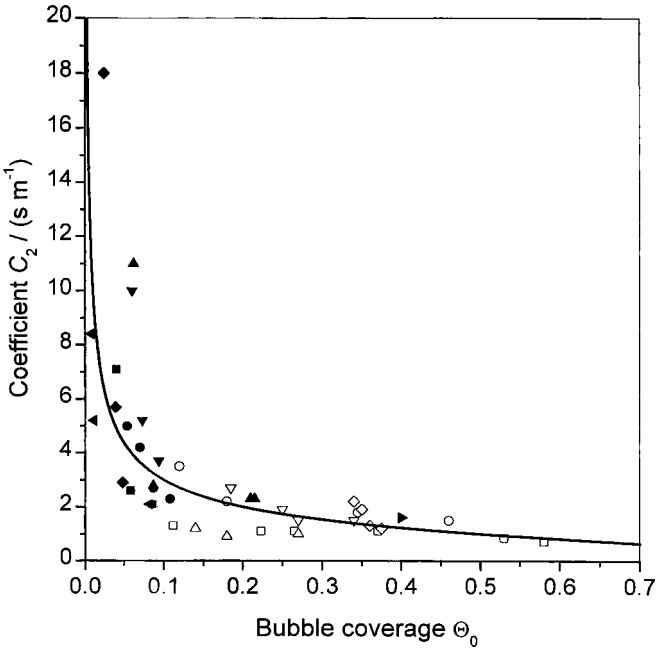

Figure 7. Coefficient C_2 in Eq. 27 as a function of the bubble coverage, Θ_0. Hydrogen and oxygen evolution at electrodes of nickel, copper, platinum, stainless steel, and graphite. 1 M KOH at 30-34°C. (■ ● ▲ ▼ ◀ ◆) H_2 at various cathode materials, (□ ○ △ ▽ ◇) O_2 at various anode materials.

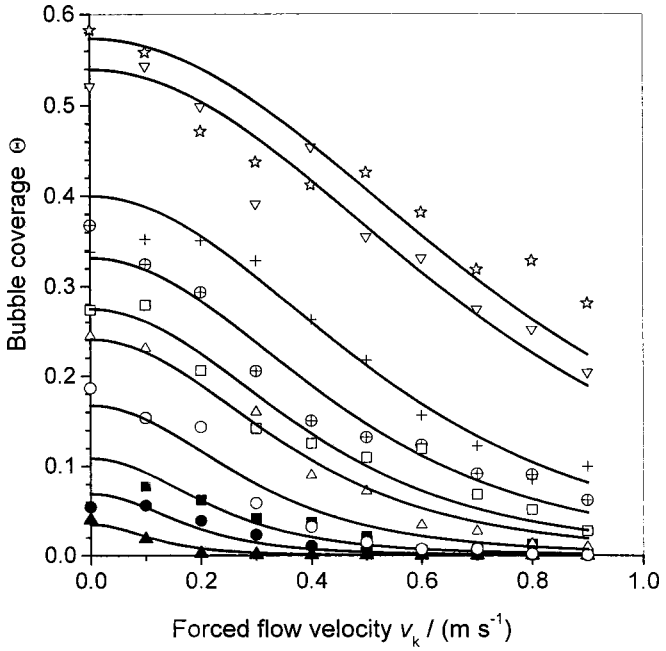

Figure 8. Effect of forced flow velocity on the bubble coverage. Hydrogen and oxygen evolution at a nickel electrode. 1 M KOH at 30-34°C. Current densities: Anode: (△) 10 A m^{-2}, (○) 20 A m^{-2}, (□) 40 A m^{-2}, (⊕) 80 A m^{-2}, (+) 160 A m^{-2}, (▽) 320 A m^{-2}, and (☆) 640 A m^{-2}. Cathode: (▲) 10 A m^{-2}, (●) 20 A m^{-2}, and (■) 40 A m^{-2}. Data correlated by Eq. 28.

$$\frac{\Theta}{\Theta_0} = \left[1 + \frac{\left(\frac{v_k}{\text{m s}^{-1}}\right)^2}{\left(\frac{1}{\Theta_0} - 1\right)^{-1} + \left(\frac{v_f}{\text{m s}^{-1}}\right)^2} \right]^{-2} \qquad [27]$$

Equation 27 gives a quantitative relationship between the actual bubble coverage and the current density and the condition and material of the electrode, expressed by Θ_0, and the velocity components of free and forced flow in vertical interelectrode gaps. However, immediate practical application is problematic for various reasons. The bubble coverage varies along the electrode height, and the variation cannot be predicted reliably at present. The unknown free flow velocity v_f is dependent not only on bubble size and liquid properties, but also and mainly on the geometry of the flow channel, *i.e.*, the interelectrode gap, and the distance from the leading channel edge as evidenced by mathematical flow simulation.[29] For practical application, it is inevitable to disregard the action of natural flow velocity v_f. Equation 27 then takes the simple and easy-to-use form

$$\frac{\Theta}{\Theta_0} = \left[1 + \left(\frac{1}{\Theta_0} - 1\right)\left(\frac{v_k}{\text{m s}^{-1}}\right)^2 \right]^{-2} \qquad [28]$$

Values of Θ_0 (for stagnant electrolyte liquid) may be estimated from Fig. 1. Experimental results are shown in Fig. 3 to 6 supporting the usefulness of Eq. 28. A compilation is given in Fig. 8.

Discussion

The comprehensive Eq. 24 and its simplified form Eq. 28 were derived for large, planar vertical electrode surfaces. In many cases, the structure of industrial electrodes is more complex, but since their microgeometry is often much larger than the size of detaching bubbles, the results may be applied, at least approximately, to these geometries, too.

In the section on Theory of flowing electrolytes, the impact of mechanical forces on the break-off diameter was analyzed. However, as seen from Eq. 2, the bubble coverage is equally affected by the bubble population density z/A. This value depends not only on the number of active nucleation sites, but also on the velocity of bubble growth which is controlled by the supersaturation of the electrolyte liquid adjacent to the electrode. But the concentration with dissolved gas is controlled by mass transfer of dissolved gas from the electrode to the liquid bulk. This mass transfer is in turn dependent on both the macroconvection induced by the flow velocity $\overline{v}$ as a complex of natural flow and forced flow, Eq. 11, and the microconvection induced by growth of adhering bubbles. We are encountered with a system of complex interactions, the extent of which cannot be assessed satisfactorily. Therefore, at present, it is inevitable to be content with partially empirical relationships. Equation 20 is a simple attempt.

The measurements further show that the bubble coverage decreases with the distance from the leading edge. An explanation would be the so-called scavenger effect.[30] Bubbles gliding along the electrode surface coalesce with bubbles they meet and form a path free of bubbles. However, it is likely that the increasing bubble accumulation near the electrode affects an enlarged free flow which is seen to intensify the shear force acting on adhering bubbles. Theoretical estimates[26] as well as mathematical flow simulations[29] confirm the formation of substantial flow velocities near the electrode as a result of the lowered effective density of the gas/liquid dispersion. They depend on the current density and on the gas flow rate which increases downstream. The variation of the velocity with the flow length is not taken into account in the present treatment. It must be concluded that for long flow lengths the values of the bubble coverage estimated from Eq. 24 or 28 are even somewhat too large.

Strictly, the value Θ_0 in Eq. 26 denotes the bubble coverage at $v_k = 0$ and arbitrary values of v_f, as seen from Eq. 23. Thus it is not identical with the value Θ_0 in Eq. 3 obtained from laboratory experiments in stagnant liquids. Since reliable data of the free flow velocity are not available, as pointed out in the section Design equation for practical application both values may be set equal for the sake of simplicity.

These are some of the reasons of the scatter seen from Fig. 3 to 8. Others are the stochastic character of bubble behavior: The size of

Downloaded on 2015-06-26 to IP 132.236.27.111 address. Redistribution subject to ECS terms of use (see ecsdl.org/site/terms_use) unless CC License in place (see abstract).

adhering bubbles varies with time and position, and the image field was chosen small (6.3×8.4 mm) to obtain sufficiently reliable information. Recirculated bubbles may have affected the quality of information, and, of course, the evaluation of the images was not perfect. Nonetheless, the analysis shows the strong effect of flow on the bubble coverage and provides insight into the complex action of forced flow on mass transfer of gas-evolving electrodes: Enhanced electrolyte flow with decrease in bubble coverage lowers the effect of microconvective mass transfer due to bubble growth and departure, but results in an increase in macroconvective mass transfer.

Conclusions

All diagrams show that the bubble coverage strongly decreases as the flow velocity past vertical electrodes increases. The flow velocity results from forced flow through the electrode/membrane gap superimposed by natural flow induced by the two-phase flow of the gas-in-liquid dispersion. For estimates of mass transfer and current distribution in industrial flow-through cells with vertical electrodes, the discrepancy of the actual bubble coverage from that of stagnant liquids must be taken into account.

For practical estimates of the bubble coverage of vertical gas-evolving electrodes, the simplified Eq. 28 together with Eq. 3 is recommended.

List of Symbols

A electrode surface area, m^2
C_1 parameter Eq. 8, kg m s^{-2}
C_2 parameter Eq. 17, s^2 m^{-2}
C_3 parameter Eq. 18
C_4 parameter Eq. 20, m^2
d bubble break-off diameter, m
F force, kg m s^{-2}
g acceleration due to gravity, m s^{-2}
I current, A
K_1 numerical constant Eq. 1, -
K_2 numerical constant Eq. 6, -
m exponent, Eq. 8
n exponent, Eq. 20
R bubble radius, m
R_r radius of detaching bubble, m
S cross-sectional area, m^2
t_r residence time, s
V volume of adhering bubble, m^3
$\dot{V}_L$ volume flow rate of liquid, m^3 s^{-1}
v^* average flow velocity at adhering bubble, m s^{-1}
v_{max} maximum flow velocity in channel, m s^{-1}
$\overline{v}$ average flow velocity in channel Eq. 11, m s^{-1}
v_f free flow velocity, m s^{-1}
v_k forced flow velocity, m s^{-1}
Y interelectrode distance, m
y coordinate normal to main flow direction, m
z number of adhering bubbles

Greek

γ surface tension, kg s^{-2}
ϑ contact angle
ζ drag number
Θ fractional bubble coverage of the electrode surface, -
Θ_0 fractional bubble coverage for zero forced flow, -
ρ_G gas density, kg m^{-3}
ρ_L liquid density, kg m^{-3}

References

1. H. Vogt, in *Comprehensive Treatise of Electrochemistry*, E. Yeager, J. O'M. Bockris, B. E. Conway, and S. Sarangapani, Editors, p. 455, Vol. 6, Plenum, New York (1983).
2. C. W. M. P. Sillen, Doctoral dissertation, Technische Hogeschool, Eindhoven, The Netherlands (1983).
3. L. J. J. Janssen, C. W. M. P. Sillen, E. Barendrecht, and S. J. D. van Stralen, *Electrochim. Acta*, **29**, 633 (1984).
4. J. Eigeldinger and H. Vogt, *Electrochim. Acta*, **5**, 4449 (2000).
5. J. Venczel, Doctoral dissertation, Swiss Federal Institute of Technology, Eidgenössische Techniche Hochschule, Zurich, Switzerland (1961).
6. H. Vogt, *Electrochim. Acta*, **25**, 527 (1980).
7. P. J. Sides and C. W. Tobias, *J. Electrochem. Soc.*, **127**, 288 (1980).
8. M. Krenz, L. Müller, and A. Pomp, *Electrochim. Acta*, **31**, 723 (1986).
9. J. Dukovic and C. W. Tobias, *J. Electrochem. Soc.*, **134**, 331 (1987).
10. H. Vogt, *Electrochim. Acta*, **42**, 2695 (1997).
11. E. Baars and C. Kayser, *Z. Elektrochem.*, **36**, 428 (1930).
12. B. Kabanow and A. Frumkin, *Z. Phys. Chem. Abt. A*, **165**, 433 (1933); B. Kabanow and A. Frumkin, *Z. Phys. Chem. Abt. A*, **166**, 316 (1933).
13. R. Darby and M. S. Haque, *Chem. Eng. Sci.*, **28**, 1129 (1973).
14. L. J. J. Janssen and S. J. D. van Stralen, *Electrochim. Acta*, **26**, 1011 (1981).
15. R. Kind, Doctoral dissertation, Swiss Federal Institute of Technology, Eidgenössische Technische Hochschule, Zürich, Switzerland (1975).
16. M. Krenz, Doctoral Dissertation A, Humboldt-Universität, Berlin (1984).
17. A. W. Bryson and D. L. Hofman, *J. Appl. Electrochem.*, **19**, 116 (1989).
18. L. Müller, H.-J. Heidrich, and B. Schultz, *Z. Chem.*, **30**, 81 (1990).
19. H. Riegel, *Einfluß von Blasenwachstum und Zweiphasenströmung auf die elektrolytische Erzeugung von Wasserstoff*, Fortschritts-Berichte des VDI, VDI-Verlag, Düsseldorf (1997).
20. P. V. Polyakov, V. M. Mozhaev, V. V. Burnakin, V. A. Kryukovskii, and V. E. Nikolaenko, *Tsvetnye Met.*, **52**, 55 (1979); *Sov. J. Non-Ferrous Met.*, **20**, 46 (1979).
21. H. Vogt, *Electrochemical Reactors with Gas Evolution*, Vol. 20, VDI-Verlag, Düsseldorf, p. 369 (1982).
22. R. A. M. Al-Hayes and R. H. S. Winterton, *PCH, PhysicoChem. Hydrodyn.*, **4**, 221 (1983).
23. N. Ibl, E. Adam, J. Venczel, and E. Schalch, *Chem.-Ing.-Tech.*, **43**, 202 (1971).
24. L. Sigrist, O. Dossenbach, and N. Ibl, *J. Appl. Electrochem.*, **10**, 223 (1980).
25. G. M. Whitney and C. W. Tobias, *AIChE J.*, **34**, 1981 (1988).
26. H. Vogt, *PCH, PhysicoChem. Hydrodyn.*, **8**, 373 (1987).
27. H. Riegel, J. Mitrović, and K. Stephan, *J. Appl. Electrochem.*, **28**, 10 (1998).
28. H. Vogt, *J. Appl. Electrochem.*, **29**, 1155 (1999).
29. M. Raja, H.-D. Kleinschrodt, and H. Vogt, in *The 19th CAD-FEM Users Meeting 2001*, the International Congress on FEM Technology, Vol. 1, no. 1.6.11 (2001).
30. P. J. Sides and C. W. Tobias, *J. Electrochem. Soc.*, **132**, 583 (1985).

Downloaded on 2015-06-26 to IP 132.236.27.111 address. Redistribution subject to ECS terms of use (see ecsdl.org/site/terms_use) unless CC License in place (see abstract).